Complexation of the Lowest Generation Poly(amidoamine)-NH_2 Dendrimers with Metal Ions, Metal Atoms, and Cu(II) Hydrates: An ab Initio Study

Francisco Tarazona-Vasquez and Perla B. Balbuena*

Department of Chemical Engineering, University of South Carolina, Columbia, South Carolina 29208

Received: February 14, 2004; In Final Form: July 1, 2004

A structural and thermodynamical characterization of complexation of poly(amidoamine) dendrimers with metal ions, metal atoms, and copper hydrates is carried out using ab initio (Hartree−Fock and density functional theory) techniques. Three binding sites (core, amide, and amine) are identified and the binding energies for attachment of naked Cu(II), Pt(II), Au(III), and Ag(I), as well as those of Cu, Pt, Au, and Ag to each of these sites are reported for PAMAM G0-NH_2. Metal ions are tetracoordinated to the core site atoms, and three types of ion-amide site coordination are found: tetracoordinated for Ag(I), tridentate for Pt(II) and bidentate for Cu(II) and Au(III). A cooperative effect between amide and amine sites is found in the bidentate coordination of ions to amide and amine N atoms; for the metal atoms such coordination becomes monodentate (to the amine N). Metal atoms form bidentate (Pt, Cu, Ag), or monodentate (Au) complexes to the core and amide sites. A Cu(II) ion solvated with one water molecule retains its bidentate coordination to the amide site while keeping its strong interaction with the water oxygen, whereas a slightly weaker binding complex is formed between doubly hydrated Cu(II) and one of the amide oxygen atoms. The thermodynamics of Cu(II) hydration by 1 to 10 water molecules is compared with those of displacement complexation reactions where Cu^{2+} in various degrees of hydration reacts with a G0-NH_2 dendrimer in gas phase.

Introduction

Dendrimers are a novel class of macromolecules that have recently generated a great deal of attention, mainly due to their potential as templates for controlled fabrication of nanosize metal particles for uses in catalysis and for electronic devices with specific functions that take advantage of their energy-harvesting and light emitting properties.[1−13] Research related to nanoparticle formation inside dendrimers has focused on achieving controlled synthesis,[4,8,14,15] optimizing the several stages that go from ion complexation,[7,9,16] through reduction,[3,4] and finally to nucleation[4,17] of the metal atoms.

The first stage, ion complexation, is crucial because it will ultimately determine where the nucleation sites would be more likely to be found. Competition between the most favorable complexation sites would also be a driving force for internal migration of the guest atoms.[1] Characterizing affinity of metal ions to the dendrimer sites is also important in relation to ion exchange and formation of bimetallic particles,[3,9,18] as well as for their potential as chelating agents.[19] However, clear identification of the nature of complexation forces and that of the geometry of the ion (metal atom)/dendrimer complex as a function of the ion (metal atom) electronic structure, as well as details of metal complexation in aqueous solutions, are still debated.[7,16,20,21]

Low-generation dendrimers have proven to be useful templating agents by providing reactive sites at their periphery.[22] On the other hand, because of their intrinsic nature, dendrimers are prone to be studied sequentially, and careful investigations involving the lowest generations may provide valuable details about the mechanisms of ion and metal attachment to the dendrimer sites.[23−25] Characterization of ion (metal atom) complexation and identification of the main adsorption sites has been carried out using mass spectrometry,[16] electron paramagnetic resonance,[18,20] UV and visible absorption spectroscopy,[7] and NMR methods,[21] among others. Molecular modeling studies including classical molecular dynamics (MD)[15,26−28] as well as coarse-grained methods[29,30] have been oriented to determine structural and dynamical aspects of high order generation dendrimers (usually G4 and higher) and their intermolecular interactions in solution, whereas only a few quantum density functional theory (DFT) studies have addressed some structural and electronic aspects of low order generation dendrimers,[31] and a first-principles study of ion complexation to dendrimers, providing detailed information about the nature of the metal ion attachment to the dendrimer sites and how the electronic and structural environment of the macromolecule changes as the ion is reduced, is not yet available. Such information can contribute to a rational design and control of metal nanoparticle fabrication inside dendrimers.

We report a systematic ab initio study of the interactions of the lowest generation poly(amidoamine) G0 dendrimers (Scheme 1) with naked metal ions and neutral metal atoms and with solvated ions. Our objective is to achieve a thorough understanding of the geometrical and electronic characteristics of ion and metal-atom complexation to the most favorable dendrimer sites that would help to rationalize the results from analytical techniques, hopefully assisting to the synthesis and fabrication of nanoparticles using dendrimers as templates. We report energetic and structural properties of ion complexation and metal adsorption for naked Cu(II), Pt(II), Au(III), and Ag(I), and Cu, Pt, Au, and Ag bound to the main adsorption sites of G0-NH_2. In this step, we assume that only cations are adsorbed inside of the dendrimer structure; this is one of the primary effects we want to capture in this study, which is the first of a series where

* Corresponding author. Current address: Department of Chemical Engineering, Texas A&M University, College Station, TX 77843. E-mail: balbuena@tamu.edu

10.1021/jp049324q CCC: $27.50
Published on Web 09/15/2004

SCHEME 1

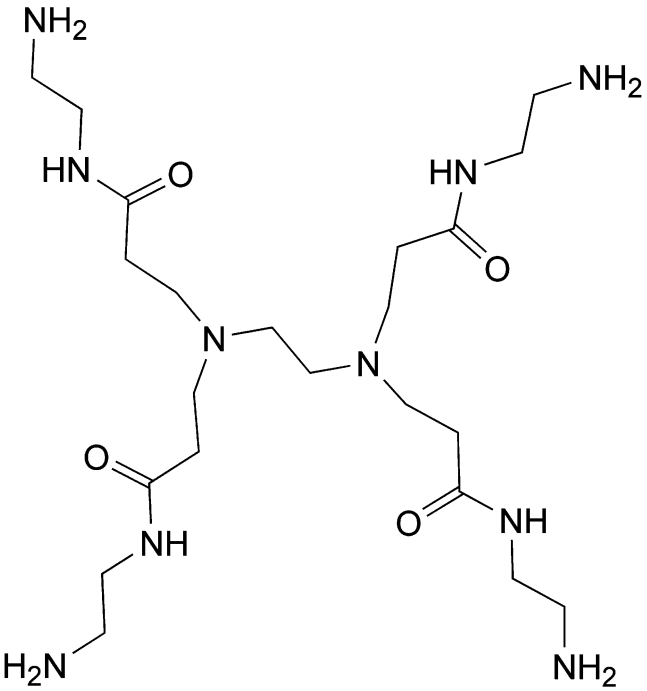

we sequentially add complexity to the system. In the last section, we attempt to address questions inferred primarily from EPR studies that suggest the existence of solvent−ion−dendrimer complexes. Thus, we investigate solvent effects on the complexation reaction by analyzing the thermodynamics of Cu^{2+} hydration in gas phase, along with that of displacement complexation reactions where a G0-NH_2 molecule reacts with Cu^{2+} in various degrees of hydration.

Methodology

Impressive advances in computer hardware and the development of efficient algorithms during the past decade have permitted the application of quantum chemical calculations to macromolecules, as recently reviewed.[32] The particular structural nature of dendrimers presents, as discussed in the Introduction, a significant advantage: the analyses of fragments and low-generation dendrimers allow the application of systematic procedures, where building blocks are added sequentially, emulating the experimental synthesis methodologies. Ion and metal atom complexation between the main adsorption sites of PAMAM G0-NH_2 (in a vacuum) and naked Cu(II), Pt(II), Au(III), and Ag(I), and Cu, Pt, Au, and Ag are investigated via a sequential approach using dendrimer fragments of increasing complexity. Full geometry optimization of complexation reactions are implemented at the HF/3-21G and HF/6-31G(d) levels of theory, existence of true local minima is tested in all cases, and binding energies are determined through hybrid DFT single point calculations on the HF fully optimized geometries. For the weak metal-atom/dendrimer site interactions, full optimizations are done with B3LYP/6-31G(d).

The 3-21G and 6-31G(d) basis sets are used for every light atom (C, N, O, H) belonging to the dendrimer, along with a relativistic effective core potential basis set with pseudopotentials for transition metals, LANL2DZ.[33] The interactions of ions and metal atoms with one dendrimer branch and those with a dendrimer fragment containing two branches are successively analyzed, taking advantage of the symmetry of the dendrimer. Counterions were not added to the model systems because our first interest is on the analysis of the complex dendrimer−cation and dendrimer−metal atom, which have been identified experimentally in dendrimer solutions where Cu salts were added.[18,20]

Various initial conformations are tested in search of alternative local minima. Second derivatives of the energy were calculated at the optimized geometries to establish the nature of the minima found as well as to obtain the zero point energy (ZPE) corrections scaled according to recommended correction factors.[34] To obtain more accurate binding energies, single point calculations are performed using a higher level method, B3LYP/6-31G(d)//HF/3-21G. By doing this, it is assumed that the geometries of the structures are well represented by HF/3-21G optimizations, as suggested by our analysis of bond lengths, bond angles, and dihedrals.[35] In addition, binding energies for the weak interactions (metal-atom/dendrimer sites) are obtained from full DFT optimizations.

Solvent effects are addressed through additional optimizations and thermochemistry calculations of the Cu(II) hydration reaction with 1 to 10 water molecules, which is compared with displacement reactions where $[Cu(H_2O)_n]^{2+}$ reacts with G0NH_2, becoming attached to the dendrimer in various degrees of hydration. Geometries of reactants and products of the displacement reactions are obtained at HF/3-21G, whereas changes of Gibbs free energy, enthalpy, and entropy of reaction result from B3LYP/6-31G(d)//HF/3-21G. All the calculations were performed using the Gaussian98 program.[36]

Results and Discussion

Complexation of Metal Atoms and Metal Ions to Various Dendrimer Sites. The feasibility of dendrimer encapsulated nanoparticle synthesis starting from ion complexation, as well as that of catalysis on those nanoparticles, was extensively demonstrated by several groups;[1−4,11,37] reported findings include synthesis of and catalysis on bimetallic nanoparticles.[38] Here we focus on complexation of Cu, Cu(II), Ag, Ag(I), Au, Au(III), Pt and Pt(II); these atoms and ions are currently being tested experimentally as seeds for the formation of catalytic metal nanoparticles.[21,39] As discussed in our related investigation of the lowest energy PAMAM G0-NH_2 conformers,[35] the atomic charge distribution indicates differences in electronegativity which determines the presence of regions with high electron density where a positively charged ion could be able to attach and bind. Our objective is to achieve a comparative analysis of the attachment of these species to the three G0 complexation sites: the core site, the secondary amide group in each branch, and the terminal amine at the end of each dendron.

The first case studied involves a G0 branch bound to the EDA core molecule, after removing the other three branches and substituting them by hydrogen atoms. This structure was used as reference for the calculation of binding energies to the amide and amine sites. Binding energies were obtained as the difference

$$\begin{aligned}\text{Binding Energy} = {} & [\text{Energy} + \text{ZPE of complex branch/ion (metal)}] - \\ & [(\text{Energy ion (metal)}) + (\text{Energy} + \\ & \text{ZPE of reference fragment (branch)})] \quad (1)\end{aligned}$$

The structure in Figure 1 was optimized (HF/3-21G for ions and B3LYP/6-31G(d) for metal atoms) and characterized as a stationary point using a second derivative calculation. Then, successive simulations were performed where a Cu ion was located next to one of the complexation regions (amide functional group, and terminal amine); the complex fragment-

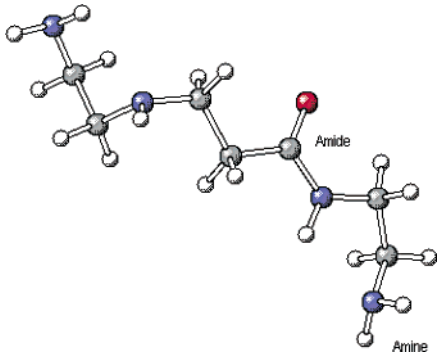

Figure 1. One branch-core system and location of tested complexation sites.

ion was fully optimized and characterized as stable minima with second-derivative calculations that also provided the ZPE corrections. The ground-state spin multiplicity (m) is listed in Table 1 for each case; in all cases the spin multiplicity of the complex agreed with that of the isolated ions except for Pt(II) where $m = 3$ for the ion, and $m = 1$ for the complex indicating an electronic rearrangement upon complexation, which is reflected in stronger binding energies as discussed later in this section. The methodology was repeated for the interactions of the branch/metal atom; the ground-state multiplicity for the Pt-G0NH_2 complex was different from that of the isolated Pt as found for the case of the ion ($m = 3$ for the metal atom, and $m = 1$ for the complex). Binding energies in eq 1 include ZPE corrections not only for the energy of the complex but also for the reference fragment energy. To calculate the DFT binding energy on the HF optimized geometries, we used the scaled ZPEs corresponding to HF/3-21G.[34]

The first point illustrated by Table 1 is the significant difference between the binding energy for the ions and those for the corresponding neutral metal atoms. The tendency observed in the binding energies (0 K, gas phase) of the ions follows the expected order of the formal charges, reflecting the role of the strong Coulombic interactions that each ion exerts over its environment. A second point is given by the DFT results from the one-branch model (Table 1), which does not include the core site, showing that the preferential site (bold values in the tables) for binding of naked ions is the amine site, that utters on the importance of the nature of the terminal functional groups in the location of nanoparticles and their stabilization either inside or outside the dendrimer, as pointed out previously.[11] This competition between amine−amide (or terminal group−amide) should become more important for higher generation dendrimers, for which the core sites become harder to be accessed by the ions. Analyzing the shortest guest−host distances and the charge distribution on these sites, we detect a bidentate coordination of the ions to two N atoms (amine and amide) found in the amine site (not shown; charges and geometries from the one-branch analysis are provided as Supporting Information). An exception is the case of Au(III) that does not attach to the amine site, becoming coordinated with the amide N atom instead.

For metal atoms, the interaction strength (Table 1) decreases in the order: Pt > Cu > Au > Ag, for both sites. In the amine site (Tables in Supporting Information), all the metal atoms coordinate primarily with the amine N atom (at distances in the order of 2 to 2.5 Å), and second with the amide N (distances in the order of 3 to 3.4 Å). This is another important and novel finding: a cooperative effect between the amide and amine sites makes a stronger ion/dendrimer binding than that found by the attachment of the ion to just one of the sites (amide). In addition, the results in Table 1 may suggest that having an interactive metal−amine terminal group stronger than that of metal−amide O may hinder the traveling of a reduced metal atom toward interior sites such as tertiary amines located at the branching points, or eventually to the dendrimer core where it is supposed that the voids are larger to hold nanoparticles of suitable size. However, it is unlikely that the metal atom binds only to one amide O as found in the one-branch calculation ion−amide site, and as a result the binding energies for the amide site shown in Table 1 may be underestimated. For this reason, we attempted a more realistic calculation assuming that the metal atom can face at least two branches while traveling to the interior sites.

A two-branch model adds the core site and improves the representation of the amide site. The reference systems for the calculation of the binding energies for the two-branch systems shown in Figure 2 were built by removing the other two branches from the fully optimized geometry (HF/3-21G) of the most symmetric dendrimer conformer (*tttt2*), and their geometry was optimized at HF/3-21G and B3LYP/6-31G(d). Table 2 shows the binding energies for the two-branch model of Figure 2a, calculated according to eq 1, showing the preference of ions and metal atoms toward the core vs the amide site. We emphasize that since our choice of reference system is arbitrary, the reported binding energies are useful to assess only the *relative* interaction strength of attachment ion (metal atom)/dendrimer among the various ions or metal atoms; for example a positive value indicates a weak interaction, but does not necessarily imply an endothermic adsorption process. Thus, the binding energy for ions follows the order: Au(III) > Pt(II) > Cu(II) > Ag(I), where the only change with respect to the one-branch values reported in Table 1 is that Pt(II) binding is stronger than that of Cu(II) in both core and amide sites. This difference is due to the fact that the two-branch model is a better representation of the amide site, especially for a strongly interacting ion as Pt(II).

Table 3 displays binding energies for metal atoms; the interaction strength follows the same order found for the one-branch system: Pt > Cu > Au > Ag, and the core site is preferred with respect to the amide site. Comparing the results obtained from HF and DFT calculations, we observe a significant decrease in the distance metal-amide N when correlation effects are taken in account, suggesting that the amide N may play a secondary but important role in the binding. Thus, the

TABLE 1: Binding Energies (in kcal/mol) of Complexes of Ion and Metal Atom to the One-Branch Amine and Amide Sites[a]; *m* Is the Multiplicity of the Complex

	B3LYP/6-31G(d)//HF/3-21G				B3LYP/6-31G(d)//HF/3-21G			B3LYP/6-31G(d)		
ion	amide	amine	*m*	metal atom	amide	amine	m	amide	amine	*m*
Cu (II)	−320.4	**−334.1**	2	Cu	−5.1	**−9.5**	2	−6.3	**−9.4**	2
Ag (I)	−53.1	**−59.4**	1	Ag	−0.1	**−2.2**	2	−0.9	**−1.9**	2
Au (III)	−745.4	**−781.0**	3	Au	−1.6	**−8.5**	2	−2.2	**−8.1**	2
Pt (II)	−252.0	**−278.9**	1	Pt	−12.7	**−32.5**	1	−15.0	**−33.4**	1

[a] Bold font is used for the preferred binding sites.

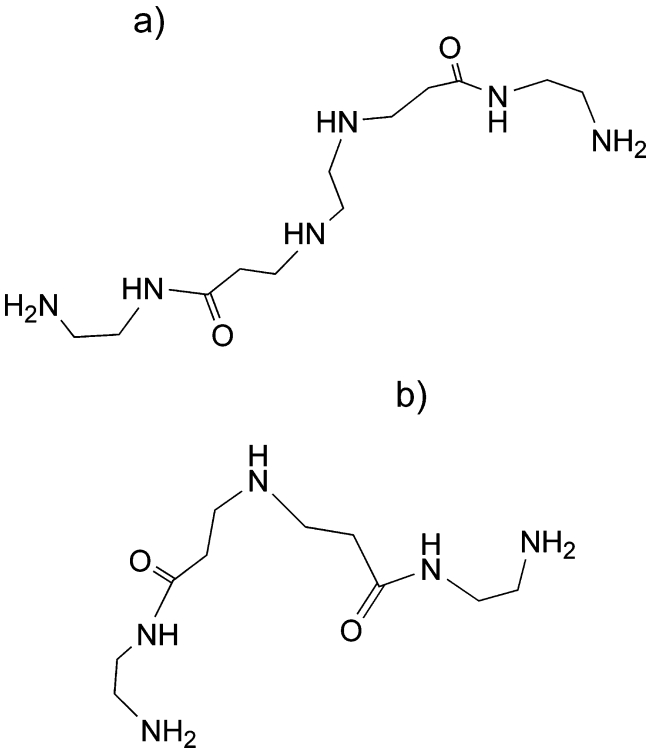

Figure 2. Structure of isolated two-branch fragments taken as reference systems for the calculation of binding energies of ion and metal atoms to the core and amide sites.

TABLE 2: Binding Energies (in kcal/mol) for Ion/Two-branch Complexes[a]

	B3LYP/6-31G(d)//HF/3-21G		B3LYP/6-31G(d)//HF/6-31G(d)	
	core	amide	core	amide
Cu (II)	**−396.2**	−377.1	**−418.8**	−375.7
Ag(I)	**−107.1**	−96.8	**−107.3**	−104.8
Au(III)	**−872.9**	−827.0	**−870.0**	−823.8
Pt(II)	**−440.2**	−390.9	**−440.3**	−391.4

[a] Bold font is used for the preferred binding sites.

TABLE 3: Binding Energies (in kcal/mol) for Metal Atom/Two-branch Complexes[a]

	B3LYP/6-31G(d)//HF/3-21G		B3LYP/6-31G(d)//HF/6-31G(d)		B3LYP/6-31G(d)	
	core	amide	core	amide	core	amide
Cu	**−8.2**	−1.1	**−11.5**	−5.1	**−11.8**	−5.7
Ag	**−1.4**	4.1	**−3.7**	−0.6	**−2.5**	−1.5
Au	**−8.3**	3.3	**−9.3**	1.0	**−12.4**	not found
Pt	**−40.3**	−38.4	**−42.9**	−37.8	**−42.4**	−38.9

[a] Bold font is used for the preferred binding sites.

amide O may be regarded as the main binding atom in this site even though the participation of the amide N in the binding cannot be minimized. Regarding the amine site, DFT results provided as Supporting Information indicate that when electron correlation is included the metal atom moves closer to the primary amine terminal N than to the amide N. Therefore, as discussed for the one-branch case, the main binding atom in the amine site is the primary amine, followed for the amide N that also may play a role in the binding. DFT optimizations of the neutral Au atom initially located close to the core and amide sites, respectively, both resulted in configurations where the atom is primarily attached to the N atom of the core site, with binding energies of −6.3 and −12.4 kcal/mol.

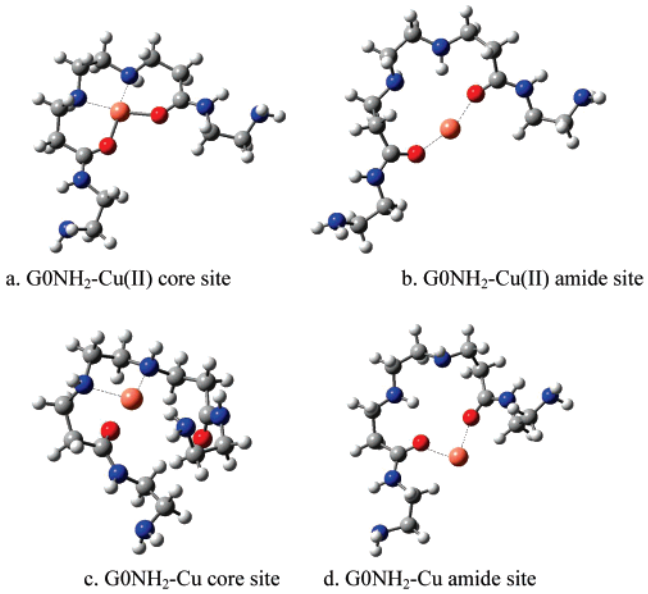

Figure 3. Optimized structures (B3LYP/6-31G(d)) of Cu(II) ion (a and b) and Cu atom (c and d) with the core and amide sites of the two branch system shown in Figure 2a, respectively.

Geometries corresponding to Cu ion and Cu atom complexation to the core and amide site are shown in Figure 3. Tables 4 and 5 extend this information, including the distances to the main atomic sites and Mulliken charges for complexation to the two-branch fragment, for all ions and metal atoms in this study. Figures 3a and b show a clear four-coordinated attachment of the ion to the core site, and a two-coordination in the amide site; whereas the interactions with neutral Cu (Figures 3c and d) are significantly weaker, as evidenced by the smaller number of host atoms located at short distances from the guest atom (Table 5). The tetradentate coordination of the ions to the core site illustrated in Figure 3a for Cu(II) is found also for the other ions (Table 4).

Table 5 illustrates a strong coordination of the neutral Cu and Ag atoms (at distances < 3 Å) with two N atoms of the core site, Pt interacts strongly with one N and one O atom, and Au is strongly connected with only one N atom in the core site. However, Table 3 indicates that Au and Cu binding energies to the core site are in the order of 10 kcal/mol; about four times lower than that of Pt attached to the core site where it is located closely to one O and one N atom. This suggests that the binding strength cannot be inferred just from geometrical considerations but is a more complex function of the dendrimer environment interacting with the foreign ion or metal atom, in particular for the metal atoms, which bear negative charges and may therefore become strongly attached to H and other positively charged atoms. We address this point further when discussing complexation to the amide site.

In the amide site (Table 4 and Figure 3b), the ions are strongly coordinated to two oxygen atoms, at an average distance of 2 Å. In addition to this double coordination, the interactions with Ag(I) and Pt(II) show also a strong coordination with two (for Ag) and one (for Pt) of the amide N atoms. Comparing Tables 4 and 5, a weaker coordination is observed for the neutral metal atoms interacting with the amide site (Table 5 and Figure 3d), their distances to the dendrimer atoms are slightly longer (0.1 to 0.3 Å) than those of the ions, the double coordination remains for Cu and it reduces from double to single coordination for Au, from four-coordinated to double-coordinated for Ag (the lowest binding energy in Table 3), and from triple to double coordination for Pt (the strongest binding energy).

TABLE 4: Ion−Core Site and Ion−Amide Site Distances (in Å) for the Two-Branch System[a]

ion/core

	M−NC		M−CO		M−O		M−N2	
site	branch 1	branch 2	branch 1	branch 2	branch 1	branch 2	branch 1	branch 2
Cu(II)	**2.11**	**2.09**	2.95	2.95	**1.94**	**1.94**	4.12	4.12
(0.65)	**(−0.61)**	**(−0.62)**	(0.65)	(0.65)	**(−0.55)**	**(−0.54)**	(−0.53)	(−0.53)
Ag(I)	**2.57**	**2.63**	3.39	3.38	**2.40**	**2.39**	4.60	4.56
(0.34)	**(−0.55)**	**(−0.54)**	(0.60)	(0.60)	**(−0.48)**	**(−0.48)**	(−0.56)	(−0.56)
Au(III)	**2.21**	**2.20**	3.06	3.26	**2.11**	**2.35**	4.25	4.51
(0.53)	**(−0.60)**	**(−0.62)**	(0.67)	(0.64)	**(−0.53)**	**(−0.45)**	(−0.54)	(−0.55)
Pt(II)	**2.06**	**2.07**	2.99	2.99	**2.05**	**2.05**	4.19	4.19
(0.60)	**(−0.66)**	**(−0.67)**	(0.66)	(0.66)	**(−0.53)**	**(−0.52)**	(−0.54)	(−0.54)

ion/amide

	M−NC		M−CO		M−O		M−N2	
site	branch 1	branch 2	branch 1	branch 2	branch 1	branch 2	branch 1	branch 2
Cu(II)	3.36	3.82	3.00	3.20	**1.95**	**2.02**	4.15	3.90
(0.45)	(−0.56)	(−0.40)	(0.62)	(0.62)	**(−0.54)**	**(−0.56)**	(−0.53)	(−0.53)
Ag(I)	**2.68**	**2.60**	3.29	3.27	**2.36**	**2.45**	4.51	4.54
(0.31)	**(−0.53)**	**(−0.54)**	(0.60)	(0.58)	**(−0.48)**	**(−0.47)**	(−0.56)	(−0.56)
Au(III)	4.35	4.35	3.46	3.47	**2.37**	**2.39**	3.96	4.05
(0.42)	(−0.42)	(−0.41)	(0.63)	(0.62)	**(−0.51)**	**(−0.54)**	(−0.53)	(−0.52)
Pt(II)	**2.04**	3.97	2.98	3.08	**2.00**	**2.01**	4.15	4.20
(0.69)	**(−0.63)**	(−0.59)	(0.66)	(0.65)	**(−0.54)**	**(−0.54)**	(−0.63)	(−0.62)

[a] HF/6-31G(d) optimized geometries, and Mulliken charges obtained from B3LYP/6-31G(d)//HF/6-31G(d). The closest interactions (distances < 3 Å) are indicated in bold. NC is the N atom in the core, CO the carbonyl C atom, O the carbonyl O atom, and N2 is the amide N atom.

TABLE 5: Distances Metal Atom−Core and Metal Atom−Amide Site (in Å) for the Two-Branch System[a]

metal/core

	M−NC		M−CO		M−O		M−N2	
site	branch 1	branch 2	branch 1	branch 2	branch 1	branch 2	branch 1	branch 2
Cu	**2.30**	**2.24**	3.44	3.49	3.80	3.85	3.87	3.83
(−0.39)	**(−0.54)**	**(−0.56)**	(0.58)	(0.58)	(−0.50)	(−0.49)	(−0.58)	(−0.57)
Ag	**2.70**	**2.69**	3.64	3.54	4.12	3.65	3.71	3.85
(−0.34)	**(−0.52)**	**(−0.52)**	(0.59)	(0.59)	(−0.51)	(−0.49)	(−0.58)	(−0.57)
Au	3.07	**2.42**	4.12	3.44	4.43	3.77	4.21	3.76
(−0.41)	(−0.51)	**(−0.52)**	(0.60)	(0.59)	(−0.51)	(−0.49)	(−0.58)	(−0.57)
Pt	**2.10**	3.11	3.34	2.31	3.72	**2.10**	3.72	3.20
(−0.33)	**(−0.64)**	(−0.56)	(0.59)	(0.51)	(−0.49)	**(−0.52)**	(−0.55)	(−0.55)

metal/amide

	M−NC		M−CO		M−O		M−N2	
site	branch 1	branch 2	branch 1	branch 2	branch 1	branch 2	branch 1	branch 2
Cu	4.36	4.92	3.13	3.23	**2.27**	**2.18**	3.74	3.71
(−0.29)	(−0.56)	(−0.53)	(0.60)	(0.60)	**(−0.49)**	**(−0.46)**	(−0.56)	(−0.57)
Ag	4.61	5.03	3.57	3.74	**2.71**	**2.68**	4.13	4.22
(−0.22)	(−0.57)	(−0.56)	(0.59)	(0.58)	**(−0.48)**	**(−0.47)**	(−0.57)	(−0.58)
Au[b]	5.99	6.42	3.95	5.68	**2.99**	6.36	5.05	5.17
(−0.12)	(−0.54)	(−0.55)	(0.56)	(0.54)	**(−0.45)**	(−0.48)	(−0.57)	(−0.57)
Pt	4.44	4.08	3.04	3.02	**2.06**	**2.04**	4.25	4.22
(−0.34)	(−0.54)	(−0.53)	(0.62)	(0.61)	**(−0.50)**	**(−0.50)**	(−0.58)	(−0.58)

[a] Optimized geometries and Mulliken charges obtained from B3LYP/6-31G(d). NC is the N atom in the core, CO the carbonyl C atom, O the carbonyl O atom, and N2 is the amide N atom. [b] HF/6-31G(d) optimized geometries, and Mulliken charges obtained from B3LYP/6-31G(d)//HF/6-31G(d)

An additional two-branch fragment, $RCOCH_2CH_2NHCH_2CH_2COR$, was investigated as shown in Figure 2b. For this fragment, the Cu(II) binding energy (B3LYP/6-31G(d)) to the core site is −383.8 kcal/mol (compared to −417.7 kcal/mol found for the other fragment using the same method), and it is found that this is the preferred binding site. For neutral Cu, two configurations are found with binding energies (B3LYP/6-31G(d)) of −10.4 and −7.1 kcal/mol, respectively; the second corresponds to the metal atom located in the same place where the ion becomes coordinated to three atoms: the branching N and two amide O atoms of the adjacent branches extending from it. The most stable configuration corresponds to Cu attached to two N atoms: one N at the branching point and a terminal primary amine N. It is important to notice that one amide O is also relatively close to the metal atom in this configuration and it may play an additional role in this binding. The small difference in energy between this stable configuration and the four-coordinated binding found for the other 2-branch fragment (−10.4 kcal/mol vs. −11.8 kcal/mol, Table 3) can be attributed to several factors, and it is really difficult to assess if differences in coordination between the four-coordinated core site (two core N and two amide O) and the new fragment site (two N and one amide O) can be the cause of the difference in binding strength. Additional information for the second 2-branch fragment,

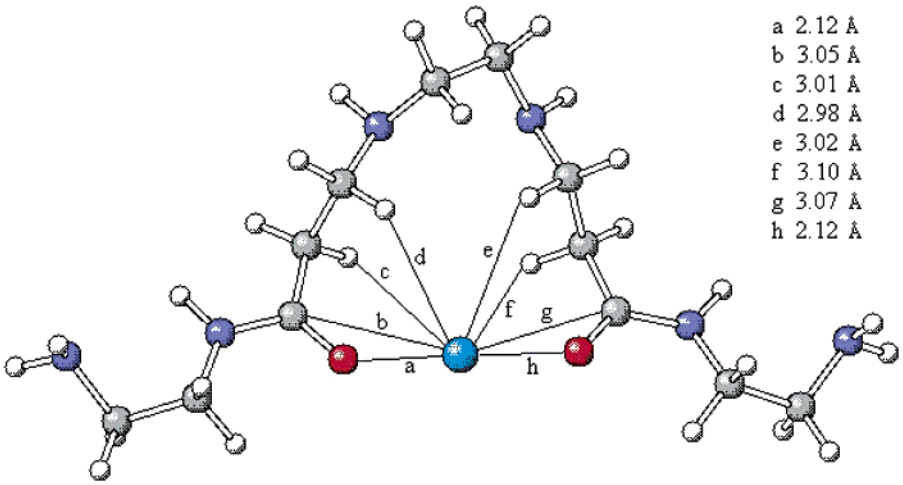

Figure 4. Optimized structure (HF/6-31G(d)) of Pt attached to the amide site, two-branch model of PAMAM G0-NH_2. $[Cu(G0\text{-}NH_2)]^{2+}$, $[Cu(G0\text{-}NH_2)\ H_2O]^{2+}$, $[Cu(G0\text{-}NH_2)(H_2O)_2]^{2+}$.

regarding charges and distances, is included as Supporting Information.

The atomic charge distribution when a metal ion or atom interacts with the two-branch structure shown in Tables 4 and 5, respectively, indicates that electron transfer occurs from the dendrimer atoms toward the guest ion or atom. We emphasize that the atomic charges assigned from the Mulliken population analysis provide qualitative information about the spatial distribution of the electronic density; the atomic charges (which are not physical observables) are the result of an approximate partition of the calculated electronic density; however, they provide valuable insights about such distribution that helps in the interpretation of the complexation process. In both cases (ion and metal atom), the extent of charge transfer depends on the electron affinities and polarizabilities of both the ion and ligand atoms (dendrimer branches).[40] To illustrate this point, Figure 4 shows the attachment of Pt neutral to the amide site, where it is located equidistant (at 2.12 Å) from the two amide O atoms, and the presence of a micropolarized environment shown by its coordination (at 3 Å) with four H atoms each belonging to a CH_2 group and with two C atoms of the carbonyl groups. Thus, although both the neutral guest atom and the two amide O atoms are negatively charged, they are surrounded by a positively charged environment that stabilizes the complex.

Results from this research show clear differences in the complexation of naked ions (metal atoms) to the dendrimer sites. Metal ions are tetracoordinated to the core site atoms, and three types of ion−amide site coordination are found: tetradentate for Ag(I), tridentate for Pt(II), and bidentate for Cu(II) and Au-(III). Metal atoms form bidentate (Pt, Cu, Ag) or monodentate (Au) complexes to the core site, and monodentate (Au) or bidentate (Pt, Cu, Ag) to the amide site. These conclusions are consistent with experimental findings, which have proposed the existence of naked Cu(II) ions in a tetragonal ligand field, most likely bonded to two tertiary amines (core) and two other N- or O-containing ligands.[4,7,16,19] Other researchers have discussed the difficulty to prepare stable Ag[9] and Au[17] nanoparticles due to the low ability of Ag and Au to keep stable composites inside dendrimers, which may be explained by the low binding energy of these metal atoms to dendrimer sites. Successful Ag-dendrimer composites have been reported using other techniques such as photolysis to aid in the reduction process;[18] which points to the need of appropriate preparation procedures to overcome the relatively low affinity of these metal atoms to the dendrimer sites. Another finding of this section (not yet detected experimentally) refers to a cooperative effect found in the bidentate coordination of ions to the amine and amide N atoms, which has a stronger binding energy than that to the amide oxygen. After reduction, the neutral atoms become primarily attached to the amide N atom, with a slightly weaker connection to the amine N, but still showing higher binding energy than the complexation to the amide O atom ("pure" amide site). Thus, the role of the terminal groups may be to act as a first strong attraction point that facilitates further interactions with interior sites. Finally, in relation to metal−atom complexation, we emphasize the development of a micropolarized environment triggered by an initial guest−host (O−Pt in Figure 4) electron transfer where several of the positively charged atoms help to create an electrostatic field that keeps the metal atom bound to the site. Such description has a close resemblance with metal complexes found in biological systems.[41] In the next section, we examine the solvent effect on complexation by investigating the attachment of hydrated Cu ions to the G0 amide site. Thus, we first compare/test our results of the two-branch system with those of the complete G0 for naked Cu(II), and then we analyze the effect of water molecules in the complexation process for hydrated Cu(II) with the amide site of G0-NH_2.

Thermodynamics of Cu(II) Hydration and Complexation of Cu(II) Mono- and Bihydrates with PAMAM-G0-NH_2. Studies of the thermodynamics of Cu(II) hydration and that of complexation of the ion to a G0 amide site were carried out at the HF/3-21G and B3LYP/6-31G(d)//HF/3-21G levels; the complexation reactions were investigated for the complete dendrimer interacting with Cu(II) at various hydration levels. Results for G0-NH_2 (*tttt1* conformation) were used in these calculations. Reported energy values contain the thermal correction to the Gibbs free energy as calculated from frequency calculations done with the same method/basis set; all structures were characterized as stationary points with no imaginary frequencies.

We analyze the following four reactions, where n is the number of water molecules that coordinate with the ion. Reaction I ($n = 1-10$) is the Cu ion hydration reaction that involves formation of n (1 to 6) Cu−O bonds in the first shell of the Cu ion, and one to four extra water molecules in the second shell H-bonded to those in the first hydration shell:

$$Cu^{2+} + nH_2O \rightarrow [Cu(H_2O)_n]^{2+}$$

Reaction II ($n = 1-10$) is a displacement reaction involving

TABLE 6: Distances (in Å) and Charge Distribution (in e) for Cu−G0-$NH_2(H_2O)_n$ with n = 0, 1, and 2 (B3LYP/6-31G(d)//HF/3-21G)[a]

# H_2O molecules	Cu charge	M−NC		M−O		M−N2		M−OW	
		branch 1	branch 2	branch 1	branch 2	branch 1	branch 2	H_2O-1	H_2O-2
0		4.46	4.95	**1.90**	**1.91**	4.13	4.16		
	(0.47)	**(**−0.23**)**	**(**−0.38**)**	**(**−0.57**)**	**(**−0.55**)**	**(**−0.54**)**	**(**−0.54**)**		
1		4.43	5.53	**2.07**	**2.08**	3.96	4.33	**2.02**	
	(0.41)	**(**−0.26**)**	**(**−0.37**)**	**(**−0.53**)**	**(**−0.51**)**	**(**−0.54**)**	**(**−0.56**)**	**(**−0.83**)**	
2		4.69	5.63	**2.06**	3.39	3.75	5.63	**2.03**	**2.02**
	(0.35)	**(**−0.26**)**	**(**−0.37**)**	**(**−0.53**)**	**(**−0.53**)**	**(**−0.55**)**	**(**−0.56**)**	**(**−0.83**)**	**(**−0.82**)**

[a] Distances shorter than 3 Å and their corresponding charges are indicated in bold face. NC is the N atom in the core, O the carbonyl O atom, N2 the amide N atom, and OW the water oxygen atom.

the dehydration of the Cu hydrate with rupture of n (n =1−10) bonds in the Cu hydrate complex and formation of a (naked Cu)−dendrimer complex:

$$[Cu(H_2O)_n]^{2+} + G0NH_2 \rightarrow [Cu(G0\text{-}NH_2)]^{2+} + nH_2O$$

Reaction III (n = 1−10) is another displacement reaction involving the dehydration of the Cu hydrate with rupture of n−1 (n = 1−10) bonds in the Cu hydrate complex and formation of a Cu(H_2O)−dendrimer complex:

$$[Cu(H_2O)_n]^{2+} + G0NH_2 \rightarrow [Cu(H_2O)(G0\text{-}NH_2)]^{2+} + (n-1)H_2O$$

Reaction IV (n = 2−10) is a third displacement reaction involving the dehydration of the Cu hydrate with rupture of n−2 (n = 2−10) bonds in the Cu hydrate complex and formation of a Cu(H_2O)$_2$−dendrimer complex:

$$[Cu(H_2O)_n]^{2+} + G0NH_2 \rightarrow [Cu(H_2O)_2(G0\text{-}NH_2)]^{2+} + (n-2)H_2O$$

Cu(II) forms stable hydrates by reaction with 1−10 water molecules. Because of the large size of the systems involved, we report calculations using a relatively low basis set; we expect that the reported results are valid qualitatively and permit us to evaluate the relative interaction strength of the ion with the aqueous system, compared to those of the ion/dendrimer system. To assess the quality of our calculations, we compared our calculated binding energies (−121.0 and −209.2 kcal/mol, respectively) for $[Cu(H_2O)]^{2+}$ and $[Cu(H_2O)_2]^{2+}$ with those (−115.8 kcal/mol and −196.7 kcal/mol) reported in a recent DFT study using a larger basis set (B3LYP/6-311+G(d,p) for atoms and B3LYP/LANL2DZ for ions).[42] A more extensive discussion of the structure and energetics of the ion−water complexes will be reported elsewhere.

For reactions II, III, and IV it is assumed that Cu(II) is located in the amide site and coordinated with water at that site. The optimized geometries (HF/3-21G) for $[Cu(G0\text{-}NH_2)]^{2+}$, $[Cu(G0\text{-}NH_2)\ H_2O]^{2+}$, and $[Cu(G0\text{-}NH_2)(H_2O)_2]^{2+}$ are shown in Figure 5. The totally dehydrated Cu(II) shows a double coordination to oxygen atoms, as was determined from the results in Figure 3b and Table 2 from the two-branch model. Comparing the geometry and charge distribution obtained from the two-branch model to those for Cu(II) attached to the amide site of G0-NH_2 (first row of Table 6 and Figure 5, left), it is observed that the distances to and charges of the strongly interacting O are similar in both cases, confirming that our simpler model was appropriate to capture the main features of ion complexation to G0. Table 5 also displays distances and charges of the ion to its closest atomic sites for attachment of the Cu(II) mono- and bihydrates, indicating that like the naked ion, the monohydrated ion, is coordinated to two dendrimer O atoms and, in addition, to the water oxygen; the distances from the ion to the dendrimer O atoms are elongated (in 0.17 Å) with respect to the dehydrated case, whereas the Cu(II)−O_{water} distance is 0.05−0.06 Å shorter than that of the Cu(II)−$O_{dendrimer}$. The bihydrated Cu(II) coordinates with two water molecules and only one O atom of the dendrimer, becoming more separated from the second one (Figure 5, right, and Table 6). Stable complexes of Cu(II) with carboxylate groups (in half-generation polyamidoamine dendrimers) and with amino groups (in full generation dendrimers) were inferred from EPR measurements,[18,20] which also suggested the existence of Cu(II) bihydrates where Cu(II) is coordinated to two water molecules and two dendrimer sites. However, our results show some differences with those inferred from the EPR studies. In aqueous Cu^{2+} solutions, Ottaviani et al.[20] proposed the existence of complexes of (a) naked Cu^{2+} bound to two terminal primary amine groups and to two tertiary amines and (b) Cu^{2+} coordinated to two water molecules and two primary amines. The first structure seems unlikely according to our studies; instead we found naked Cu^{2+} in tetradent coordination to two

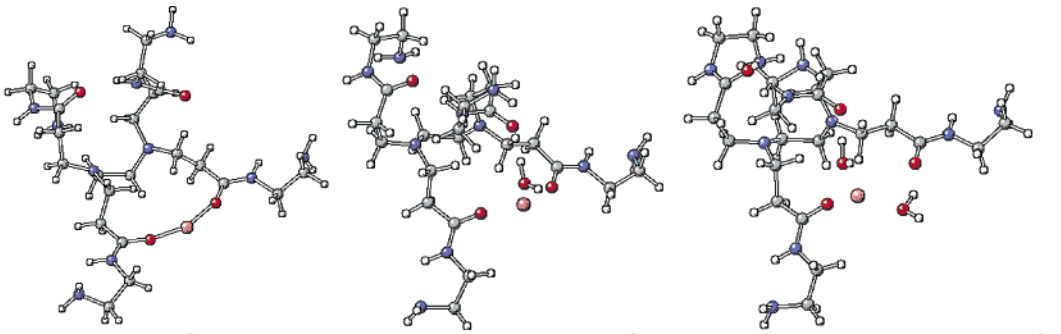

Figure 5. Optimized geometries (HF/3-21G) for complexes between water, G0-NH_2, and Cu(II).

TABLE 7: HF/3-21G and B3LYP/6-31G(d)//HF/3-21G Electronic Energies (E_{el}), Zero-Point Energies (ZPE), Enthalpy (H), and Gibbs (G) Free Energies (all in a.u.; ZPEs scaled by 0.9207[34])

	HF/3-21G				B3LYP/6-31G(d)//HF/3-21G		
species	E_{el}	ZPE	H	G	E_{el}	H	G
G0-NH2	−1695.52532	0.73885	−1694.74513	−1694.86708	−1715.64605	−1714.86585	−1714.98781
$[Cu(G0\text{-}NH_2)]^{2+}$	−1890.21885	0.74365	−1889.43317	−1889.55628	−1911.33724	−1910.55156	−1910.67467
$[Cu(G0\text{-}NH_2)H_2O]^{2+}$	−1965.86814	0.76840	−1965.05545	−1965.18065	−1987.78060	−1986.96790	−1987.09311
$[Cu(G0\text{-}NH_2)(H_2O)_2]^{2+}$	−2041.49784	0.79255	−2040.65832	−2040.79166	−2064.21878	−2063.37926	−2063.51259
$[Cu(H_2O)]^{2+}$	−269.88277	0.02422	−269.85450	−269.88345	−271.67014	−271.64186	−271.67082
$[Cu(H2O)_2]^{2+}$	−345.64030	0.04931	−345.58454	−345.61967	−348.22384	−348.16809	−348.20322
$[Cu(H_2O)_3]^{2+}$	−421.34813	0.07391	−421.26517	−421.30797	−424.73769	−424.65473	−424.69753
$[Cu(H_2O)_4]^{2+}$	−497.03339	0.09870	−496.92337	−496.97120	−501.22676	−501.11674	−501.16457
$[Cu(H_2O)_5]^{2+}$	−572.69686	0.12236	−572.56041	−572.61288	−577.68767	−577.55121	−577.60369
$[Cu(H_2O)_6]^{2+}$	−648.34251	0.14492	−648.18010	−648.23952	−654.13707	−653.97466	−654.03408
$[Cu(H_2O)_7]^{2+}$	−723.98061	0.16865	−723.79154	−723.85880	−730.58641	−730.39734	−730.46460
$[Cu(H_2O)_8]^{2+}$	−799.61607	0.19235	−799.40023	−799.47567	−807.03318	−806.81734	−806.89277
$[Cu(H_2O)_9]^{2+}$	−875.24656	0.21649	−875.00373	−875.08734	−883.47469	−883.23186	−883.31547
$[Cu(H_2O)_{10}]^{2+}$	−950.87557	0.24034	−950.60584	−950.69711	−959.91487	−959.64514	−959.73641
Cu^{2+}	−194.10679	0.00000	−194.10443	−194.12330	−195.06571	−195.06335	−195.08222
H_2O	−75.58596	0.02005	−75.56213	−75.58356	−76.40853	−76.38470	−76.40613

TABLE 8: Calculated (B3LYP/6-31G(d)//HF/3-21G and HF/3-21G) Energy Changes $\Delta E°$, Gibbs Free Energy Changes $\Delta G°$, Enthalpy Changes $\Delta H°$, and Entropy Changes $\Delta S°$ for Reactions I−IV at 298 K

	B3LYP/6-31G(d)//HF/3-21G							
	ΔE° of Reaction (kcal/mol)				$\Delta H°$ of Reaction (kcal/mol)			
n (# water molecules)	I	II	III	IV	I	II	III	IV
1	−121.0	−268.9	−288.2		−121.6	−268.9	−288.8	
2	−209.2	−180.7	−200.0	−216.1	−210.4	−180.1	−200.0	−216.7
3	−272.6	−117.3	−136.6	−152.7	−274.4	−116.1	−136.0	−152.7
4	−320.5	−69.4	−88.7	−104.8	−322.9	−67.6	−87.5	−104.2
5	−351.2	−38.8	−58.0	−74.2	−354.1	−36.4	−56.3	−73.0
6	−374.9	−15.1	−34.3	−50.4	−378.4	−12.1	−31.9	−48.7
7	−398.1	8.2	−11.1	−27.2	−402.3	11.7	−8.1	−24.8
8	−419.7	29.7	10.5	−5.7	−424.4	33.9	14.0	−2.7
9	−437.8	47.9	28.6	12.5	−443.1	52.6	32.7	16.0
10	−455.1	65.2	45.9	29.8	−461.1	70.5	50.7	33.9

	ΔG of Reaction (kcal/mol)				ΔS of Reaction (kcal/mol/K)[a]			
n (# water molecules)	I	II	III	IV	I	II	III	IV
1	−114.5	−264.9	−272.6		−0.024	−0.013	−0.054	
2	−193.7	−185.7	−193.4	−201.8	−0.056	0.019	−0.022	−0.050
3	−249.1	−130.3	−138.1	−146.5	−0.085	0.048	0.007	−0.021
4	−287.3	−92.1	−99.8	−108.2	−0.119	0.082	0.041	0.013
5	−308.0	−71.4	−79.1	−87.5	−0.155	0.117	0.077	0.049
6	−323.2	−56.2	−63.9	−72.3	−0.185	0.148	0.107	0.079
7	−338.5	−40.9	−48.6	−57.0	−0.214	0.176	0.136	0.108
8	−352.4	−27.1	−34.8	−43.2	−0.242	0.204	0.164	0.136
9	−362.8	−16.7	−24.4	−32.8	−0.270	0.232	0.192	0.164
10	−372.1	−7.4	−15.1	−23.5	−0.299	0.261	0.221	0.193

[a] ΔS is assumed to be the same as in the HF method.

core amines and two amide oxygen atoms (Figure 3a), or in bidentate coordination with two amide oxygen atoms (Figure 3b and Figure 5, left). The tetradent coordination with two N and two O atoms was proposed in a more recent EPR study[18] where complexation of both Cu^{2+} and Ag^+ atoms was investigated. The second proposed structure[20] involving Cu^{2+} solvated with two water molecules, which interact with two amine N atoms, has a correspondence with our calculated Figure 5 (right), although in this case the interaction is with two amide oxygen atoms.

Basic energetics data for all the reactions are given in Table 7 (at HF/3-21G and B3LYP/6-31G(d)//HF/3-21G levels), and thermodynamic data for the hydration and displacement reactions are presented in Table 8. Reaction I is exothermic and clearly dominated by the enthalpic contribution (Table 8), whereas the entropy of the system decreases as more water molecules are added, making the net Gibbs free energy less negative. Note also that the $\Delta\Delta G°$ needed to add a new water molecule to the hydration complex, calculated as the difference between successive values of $\Delta G°$ for the hydration reaction I, decreases in the order −79.2 kcal/mol ($n = 2$), −55.4 kcal/mol ($n = 3$), −38.2 kcal/mol ($n = 4$), −20.7 kcal/mol ($n = 5$), and −15.2 kcal/mol ($n = 6$). The energy of the $[Cu^{2+}(H_2O)_6]$ complex (calculated with the values shown in Table 6) illustrates the strong interaction between the Cu(II) ion and its first hydration shell; these values can be compared with the magnitude of the interaction Cu(II)/dendrimer sites. Thus, the calculated binding energy of a Cu(II) hexahydrate (−374.9 kcal/mol) is lower than that of a naked Cu ion attached to the amide site, in Cu(II)G0-NH_2 (−398.5 kcal/mol), whereas those of the Cu monohydrate, Cu(II)(H_2O)G0-NH_2, and bihydrate, Cu(II)-$(H_2O)_2$/G0-NH_2, are −288.1 kcal/mol and −216.2 kcal mol, respectively. The last three binding energies were calculated from the values of E_{el} and ZPE in Table 7, as the difference:

E (Cu(II)$(H_2O)_n$G0-NH_2) − E (Cu(II)$(H_2O)_n$) − E (G0-NH_2), for $n = 1$ and 2, with $E = E_{el}$ + ZPE. Cu(II) in aqueous solutions exists mostly as hexahydrate, where the water molecules in the first shell of the ion are exchanged with others from the bulk with a characteristic dynamics in the order of 100 ps.[43] Preliminary results from our molecular dynamics simulations[44] indicate that when hexahydrated Cu(II) complexes are located in the proximity of a dendrimer site, such dynamic exchange facilitates the interaction with the favorable dendrimer sites, and the formation of very stable hydrated Cu ion/dendrimer complexes.

Reactions II, III, and IV are possible displacement reactions where a completely dehydrated Cu ion (reaction II), a monohydrate ($Cu^{2+}H_2O$, reaction III), and a dihydrate ($Cu^{2+}(H_2O)_2$, reaction IV) become attached to G0-NH2, respectively. Thermodynamic data (Table 7) indicates that all reactions are possible, with increasing probability as fewer water molecules need to be extracted (i.e., fewer hydrate bonds need to be broken) from the Cu^{2+} hydrates (the most favorable process for a given n is that for reaction IV, then III, and finally II). Reactions II, III, and IV are also highly exothermic at least up to $n = 6$. The entropic contribution changes sign along a given column. For example, $\Delta S°$ is negative for reaction II for $n = 1$, indicating an entropy decrease, and becomes positive as n increases, for $n \geq 2$, since the ordered state corresponding to the hydrated complex is destroyed. Similar trends are observed for reactions III and IV.

Summarizing, the results in Table 8 clearly suggest that the dynamics of the water solution at finite temperatures will favor the removal of one, two, or even more water molecules from the first ionic hydration shell, making instantaneous configurations of the Cu-hydrate prone to react and adsorb to the dendrimer sites, as observed experimentally.[4,7,9,19] Molecular dynamics simulations are being carried out to provide further details about ion and metal atom complexation and metal particle formation inside dendrimers.[44]

Conclusions

Favored by the radial symmetry of PAMAM G0-NH_2, three regions are clearly identified where the electron density distribution favors ion complexation or metal adsorption: the core site, the amide functional group in each branch, and the terminal amine at the end of each dendron. Binding energies of naked ions to the dendrimer sites follow the trend given by their formal charges which reflects the importance of the strong Coulombic ion−ligand interactions, where a high degree of charge transfer from the negative site toward the ion is detected, which tends to decrease the positive ionic charge. Ions attach to the dendrimer core in a four-coordination mode, bound to two N and two O atoms; in the amide sites Cu(II) and Au(III) ions form bidentate complexes with two O atoms, Pt(II) complexes via two amide O and one N atom from the core, and Ag(I) is tetracoordinated to two O amide atoms and two core N atoms. A cooperative effect between amide and amine sites is found in the bidentate coordination of ions to the amine and amide N atoms, which has a stronger binding energy than that to the amide oxygen. After reduction, the neutral atoms become primarily attached to the amine N atom, with a slightly weaker connection to the amide N but still showing higher binding energy than the complexation to the amide O atom ("pure" amide site). Thus, the terminal groups may act as a first strong attraction point that facilitates further interactions with interior sites.

The strength of binding energies due to metal−dendrimer interactions suggests the order Pt > Cu > Au > Ag. Cu and Ag atoms coordinate strongly (at distances < 3 Å) with two N and one O atoms of the core site, Pt attaches to one core N and one amide O, and Au to just one N core atom. The metal atom/dendrimer binding strength cannot be inferred just from geometrical considerations but is a more complex function of the dendrimer environment interacting with the foreign ion or metal atom, in particular for the metal atoms, which bear negative charges and may therefore become strongly attached to H and other positively charged atoms.

A Cu(II) ion solvated with one water molecule retains its bidentate coordination to the amide site while keeping its strong interaction with the water oxygen, whereas a slightly weaker binding complex is formed between doubly hydrated Cu(II) and one of the amide oxygen atoms. A thermodynamic analysis of displacement reactions for the interactions of $[Cu(H_2O)_n]^{2+}$ with G0-NH_2, involving different degrees of dehydration of the n-hydrate complex, indicate that all reactions up to $n = 6$ are spontaneous (negative $\Delta G°$ of reaction) and also highly exothermic. However, the degree of exothermicity of the displacement reaction decreases in proportion to the number of Cu−H_2O bonds that need to be broken in the n-hydrate system. On the other hand, the $\Delta S°$ of reaction becomes highly positive, the system entropy increases due to the disruption of the highly ordered hydrated complex. Thus, both the energetic and the entropic terms tend to increase $\Delta G°$ of reaction monotonically as the number of Cu−H_2O bonds that need to be broken in the n-hydrate system increases. Therefore, this study demonstrates the feasibility of attachment not only of naked ions but also of hydrated ions to the dendrimer sites.

Acknowledgment. This work is supported by the National Science Foundation grant CTS-0103135. Supercomputer time granted by the National Energy Research Scientific Computing Center (NERSC), by the National Alliance for Supercomputing Applications (Grant CTS 030036), and by the DoD Major Shared Resource Centers (ARL MSRC and ASC MSRC) is gratefully acknowledged.

Supporting Information Available: Charges and geometries from the one-branch and two-branch analyses, DFT results for the amine site. This material is available free of charge via the Internet at http://pubs.acs.org.

Note Added in Proof. Regarding the strength of the binding energies of the Cu(II) and Pt(II) ions to the dendrimer sites, although we have found that high level calculations yield the order Pt(II) > Cu(II), we emphasize that in view of the sensitivity of the results to the method/basis set employed, further investigations are needed to validate this result.

References and Notes

(1) Balogh, L.; Tomalia, D. A.; Hagnauer, G. L. *Chem. Innovation* **2000**, *30*, 19.
(2) Esumi, K. *Top. Curr. Chem.* **2003**, *227*, 31.
(3) Crooks, R. M.; Lemon, B. I., III; Sun, L.; Yeung, L. K.; Zhao, M. *Top. Curr. Chem.* **2001**, *212*, 81.
(4) Balogh, L.; Tomalia, D. *J. Am. Chem. Soc.* **1998**, *120*, 7355.
(5) Sooklal, K.; Hanus, L. H.; Ploehn, H. J.; Murphy, C. J. *Adv. Mater.* **1998**, *10*, 1083.
(6) Tomalia, D. A.; Naylor, A. M.; Goddard, W. A. *Angew. Chem., Int. Ed.* **1990**, *29*, 138.
(7) Zhao, M.; Sun, L.; Crooks, R. M. *J. Am. Chem. Soc.* **1998**, *120*, 4877.
(8) Zhao, M.; Crooks, R. M. *Adv. Mater.* **1999**, *11*, 217.
(9) Zhao, M.; Crooks, R. M. *Chem. Mater.* **1999**, *11*, 3379.
(10) Zhao, M.; Crooks, R. M. *Angew. Chem., Int. Ed. Engl.* **1999**, *38*, 364.
(11) Esumi, K.; Susuki, A.; Yamahira, A.; Torigoe, K. *Langmuir* **2000**, *16*, 2604.

(12) Frechet, J. M. J. *J. Polym. Sci. Part A: Polym. Chem.* **2003**, *41*, 3713.
(13) Barron, J. A.; Bernhard, S.; Houston, P. L.; Abruna, H. D. *J. Phys. Chem. A* **2003**, *107*, 8130.
(14) Manna, A.; Imae, T.; Aoi, K.; Okada, M.; Yogo, T. *Chem. Mater.* **2001**, *13*, 1674.
(15) Naylor, A. M.; Goddard, W. A.; Kiefer, G. E.; Tomalia, D. A. *J. Am. Chem. Soc.* **1989**, *111*, 2339.
(16) Zhou, L.; Russell, D. H.; Zhao, M.; Crooks, R. M. *Macromolecules* **2001**, *34*, 3567.
(17) Wang, R.; Wang, J.; Zheng, Z.; Carducci, M. D.; Jiao, J.; Seraphin, S. *Angew. Chem., Int. Ed.* **2001**, *40*, 549.
(18) Ottaviani, M. F.; Valluzzi, R.; Balogh, L. *Macromolecules* **2002**, *35*, 5105.
(19) Diallo, M. S.; Balogh, L.; Shafagati, A.; Johnson, J. H.; Goddard, W. A.; Tomalia, D. A. *Environ. Sci. Technol.* **1999**, *33*, 820.
(20) Ottaviani, M. F.; Montalti, F.; Turro, N. J.; Tomalia, D. A. *J. Phys. Chem. B* **1997**, *101*, 158.
(21) Pellechia, P. J.; Gao, J. X.; Gu, Y. L.; Ploehn, H. J.; Murphy, C. J. *Inorg. Chem.* **2003**, *43*, 1421.
(22) Bao, C.; Jin, M.; Lu, R.; Zhang, T.; Zhao, Y. Y. *Mater. Chem. Phys.* **2003**, *81*, 160.
(23) Furer, V. L.; Kovalenko, V. I.; Vandyukov, A. E.; Majoral, J. P.; Caminade, A. M. *Spectrochim. Acta* **2002**, *58*, 2905.
(24) Kovalenko, V. I.; Furer, V. L.; Vandyukov, A. E.; Shagidullin, R. R.; Majoral, J. P.; Caminade, A. M. *J. Mol. Struct.* **2002**, *604*, 45.
(25) Cakara, D.; Kleimann, J.; Borkovec, M. *Macromolecules* **2003**, *36*, 4201.
(26) Canetta, E.; Maino, G. *Nucl. Instrum. Methods Phys. Res. B* **2004**, *213*, 71.
(27) Cagin, T.; Wang, G.; Martin, R.; Breen, N.; Goddard, W. A. *Nanotechnology* **2000**, *11*, 77.
(28) Karatasos, K.; Adolf, D. B.; Davies, G. R. *J. Chem. Phys.* **2001**, *115*, 5310.
(29) Cagin, T.; Wang, G.; Martin, R.; Zamanakos, G.; Vaidehi, N.; Mainz, D. T.; Goddard, W. A. *Comput. Theor. Polym. Sci.* **2001**, *11*, 345.
(30) Gotze, I. O.; Likos, C. N. *Macromolecules* **2003**, *36*, 8189.
(31) Lin, C.; Wu, K.; Sa, R.; Mang, C.; Liu, P.; Zhuang, B. *Chem. Phys. Lett.* **2002**, *363*, 343.
(32) Friesner, R. A.; Dunietz, B. D. *Acc. Chem. Res.* **2001**, *34*, 351.
(33) Hay, P. J.; Wadt, W. R. *J. Chem. Phys.* **1985**, *82*, 270.
(34) Scott, A. P.; Radom, L. *J. Phys. Chem.* **1996**, *100*, 16502.
(35) Tarazona-Vasquez, F.; Balbuena, P. B. *J. Phys. Chem. B* **2004**, *108*, 15982.
(36) Frisch, M. J.; Trucks, G. W.; Schlegel, H. B.; Scuseria, G. E.; Robb, M. A.; Cheeseman, J. R.; Zakrzewski, V. G.; Montgomery, J. A.; Stratmann, R. E.; Burant, J. C.; Dapprich, S.; Millam, J. M.; Daniels, A. D.; Kudin, K. N.; Strain, O. F. M. C.; Tomasi, J.; Barone, B.; Cossi, M.; Cammi, R.; Mennucci, B.; Pomelli, C.; Adamo, C.; Clifford, S.; Ochterski, J.; Petersson, G. A.; Ayala, P. Y.; Cui, Q.; Morokuma, K.; Malick, D. K.; Rabuck, A. D.; Raghavachari, K.; Foresman, J. B.; Ciolovski, J.; Ortiz, J. V.; Stefanov, V. V.; Liu, G.; Liashensko, A.; Piskorz, P.; Komaroni, I.; Gomperts, R.; Martin, R. L.; Fox, D. J.; Keith, T.; Al-Laham, M. A.; Peng, C. Y.; Nanayakkara, A.; Gonzalez, C.; Challacombe, M.; Gill, P. M. W.; Johnson, B.; Chen, W.; Wong, M. W.; Andres, J. L.; Head-Gordon, M.; Replogle, E. S.; Pople, J. A. GAUSSIAN 98, Revision A.11; Gaussian Inc.: Pittsburgh, PA, 1998.
(37) Balogh, L.; Valluzzi, R.; Laverdure, K. S.; Gido, S. P.; Hagnauer, G. L.; Tomalia, D. A. *J. Nanoparticle Res.* **1999**, *3*, 1.
(38) Chung, Y. M.; Rhee, H. K. *J. Mol. Catal. A: Chem.* **2003**, *206*, 291.
(39) Lang, H.; May, R. A.; Iversen, B. L.; Chandler, B. D. *J. Am. Chem. Soc.* **2003**, *125*, 14832.
(40) Parish, R. V. *The Metallic Elements*, 1st ed.; Longman Inc: New York, 1977.
(41) Brammer, L. *Dalton Trans.* **2003**, 3145.
(42) El-Nahas, A. M.; Tajima, N.; Hirao, K. *Chem. Phys. Lett.* **2000**, *318*, 333.
(43) Erras-Hanauer, H.; Clark, T.; Eldik, R. v. *Coord. Chem. Rev.* **2003**, *238*−*239*, 233.
(44) Tarazona-Vasquez, F.; Balbuena, P. B. 2003 AIChE National Meeting, 2003, San Francisco, CA.